Biointerface Research in Applied Chemistry
Open-Access Journal (ISSN: 2069-5837)

Article
Volume 16, Issue 1, 2026, 17
https://doi.org/10.33263/BRIAC161.017

In Vitro and *In Silico* Evaluation of Flavonoids as Human Plasma Kallikrein Inhibitors

Hassan A. Madkhali [1,*]

[1] Department of Pharmacology and Toxicology, College of Pharmacy, Prince Sattam Bin Abdulaziz University, Al-Kharj, Saudi Arabia
* Correspondence: h.madkhali2018@gmail.com;

Received: 1.09.2025; Accepted: 15.11.2025; Published: 15.02.2026

Abstract: Plasma kallikrein (PKa), a serine proteinase in the kallikrein–kinin system, is involved in vascular inflammation and edema. In this work, three natural flavonoids, Fisetin, Morin, and Rutin, were screened as prospective human plasma kallikrein inhibitors and compared to the standard drug Sebetralstat by means of integrated in vitro and in silico assays. Chromogenic assay revealed concentration-dependent inhibition of plasma Kallikrein (IC50 = 300.13 µM for Fisetin, 377.36 µM for Morin, and 566.04 µM for Rutin). Satisfactory binding energies (–9.1, –8.6, and –7.5 kcal mol^{-1} respectively) were also predicted, along with similar interaction patterns by molecular docking analyses. MD simulations demonstrated that Morin and Fisetin formed a stable complex, whereas Rutin induced local dynamic properties. The ADMET predictions revealed acceptable pharmacokinetic profiles for Fisetin and Morin, while Rutin showed low permeability. These results point to Fisetin and Morin as candidate natural scaffolds for selective inhibition of plasma kallikrein, with moderate in vitro potency but good in silico stability and pharmacokinetics. Additional confirmation in cellular models and structure-guided optimization of these flavonoid scaffolds are required to develop safer anti-inflammatory drugs that act on the kallikrein–kinin system.

Keywords: plasma kallikrein; Fisetin; Morin; Rutin; flavonoids; inflammation; in vitro; in silico.

1. Introduction

Blood coagulation and the inflammatory response are two highly controlled physiological functions necessary for homeostasis and vascular integrity. At the crossroads of these systems resides the plasma kallikrein–kinin (PKK) pathway, an enzyme cascade that generates bradykinin, a vasoactive peptide known to induce vasodilation and inflammation. While several synthetic kallikrein inhibitors have been successfully produced, naturally occurring compounds are scarce. Accordingly, the present study aims to explore the potential of selected flavonoids as natural, biocompatible inhibitors of plasma kallikrein. One of the critical mediators is plasma kallikrein (PKa), a serine protease that forms as a product of prekallikrein activation (Fletcher factor), activated by Factor XII on negatively charged surfaces [1-3].

Plasma kallikrein plays a dual role: it participates in the amplification of the intrinsic pathway of coagulation through the feedback activation of factor XII, and it cleaves high molecular weight kininogen (HMWK) to release bradykinin, which activates B2 and B1

receptors on endothelial cells, causing an increase in vascular permeability [4]. If these mechanisms are essential in vascular regulation, their excessive activation is involved in numerous pathologies. Hereditary angioedema (HAE), for example, results from a defect in the regulation of PKa, leading to excessive production of bradykinin, responsible for recurrent edema [3, 5].

Similarly, the increased activity of PKa is involved in diabetic macular edema (DME), ischemic stroke, and septic shock, through mechanisms related to capillary permeability and excessive inflammation [5-8]. The non-essential role of PKa in hemostasis makes its pharmacological inhibition safe with respect to bleeding, unlike classical anticoagulants [9]. Thus, several PKa inhibitors have been developed, notably for HAE (hereditary angioedema), including ecallantide, lanadelumab, and berotralstat, but also for other pathological contexts [10,11].

Fisetin, Morin, and Rutin are naturally occurring flavonoids with significant potential in cardiovascular health and anti-inflammatory applications. Each of these compounds has been studied for its ability to modulate inflammatory responses and could serve as effective therapeutic agents against inflammation-related conditions. Fisetin, a flavonol found in many fruits and vegetables, exhibits a range of biological activities, including anti-inflammatory effects. Its mechanism involves inhibiting pro-inflammatory enzyme activity and modulating signaling pathways such as NF-kappa B, which plays a crucial role in the inflammatory process [12]. Morin, another flavonoid, has shown promise in addressing inflammation through its antioxidant properties. While specific studies on Morin are limited in the context I have, similar flavonoids such as quercetin and kaempferol have demonstrated their ability to inhibit pro-inflammatory cytokines and affect pathways implicated in inflammatory diseases, suggesting that Morin may have comparable actions [13]. Rutin, often found in citrus fruits, apples, and buckwheat, has been recognized for its anti-inflammatory properties. It works by reducing oxidative stress, which is closely linked to inflammation, and inhibiting key inflammatory cytokines such as TNF-alpha and interleukins, thus providing a protective effect against inflammatory insult [14].

In this perspective, in vitro chromogenic enzymatic assays and in silico approaches allow for the acceleration of the discovery of new inhibitors. In vitro chromogenic enzymatic assays provide data with high sensitivity and specificity [15]. These assays enable researchers to measure and quantify enzyme activity accurately. The analysis of frontier molecular orbitals (HOMO-LUMO), electrostatic potential maps (ESP), non-covalent interactions (NCI), combined with molecular docking, molecular dynamics (MD) simulations, and ADMET (Absorption, Distribution, Metabolism, Excretion, and Toxicity) screening, allows for a rational selection of candidates [16]. This strategy has enabled the identification of active compounds with favorable pharmacokinetic properties, reinforcing the potential of plasma kallikrein as a therapeutic target for thrombo-inflammatory diseases. Therefore, in the present study, we aimed to assess the possible inhibitory effects of selected flavonoids that have shown anti-inflammatory benefits, Fisetin, Morin, and Rutin, on plasma kallikrein activity to explore the possible impact on the management of plasma kallikrein-related disorders.

A number of synthetic inhibitors of plasma kallikrein are undergoing clinical or pre-clinical investigation, including ecallantide, lanadelumab, and berotralstat. Moreover, some natural molecules—specifically polyphenols and flavonoids such as quercetin, kaempferol, and curcumin—have been found to modulate kallikrein through antioxidant and anti-inflammatory

mechanisms partially. Such reports justify ongoing interest in the search for natural scaffolds as safer, chemically diverse inhibitors of plasma kallikrein [2,17].

Although significant progress has been made in the design of synthetic plasma kallikrein inhibitors, their use remains restricted by cost, short half-life, and off-target effects. This underscores the need for safer, easier-to-use options that possess both anti-inflammatory and anticoagulatory effects. In this regard, the present study aims at overcoming the paucity of naturally occurring inhibitors of plasma kallikrein by assessing the inhibitory potential of three commercially available flavonoids, i.e., Fisetin, Morin, and Rutin, by a combined in vitro and in silico strategy. Such natural scaffolds might have potential as modulators of kallikrein activity and, in turn, may be useful for the treatment of kallikrein-mediated diseases.

2. Materials and Methods

2.1. In vitro plasma kallikrein chromogenic assay.

Plasma kallikrein (Enzyme Research Laboratories, South Bend, IN, USA), chromogenic substrate S-2302 (Aniara, Mason, OH, USA), and Flavonoids Fisetin, Morin, and Rutin (≥ 98% purity, Sigma–Aldrich, USA) were used. Sebetralstat, a selective plasma kallikrein inhibitor, was purchased from MedChemExpress (MCE, Monmouth Junction, NJ, USA). All reagents were of analytical grade.

The inhibitory efficacies of the three flavonoids (Fisetin, Morin, and Rutin) from nature were determined using chromogenic assay against plasma kallikrein. The synthetic inhibitor Sebetralstat was used as a reference compound. Excess enzyme was stored on ice when not in use to prevent premature activation, and sterile pipette tips were used throughout to prevent contamination.

Plasma kallikrein-selective chromogenic substrate S-2302 (0.5 mM) was incubated with 2 nM of enzyme in a total reaction volume of 330 µL and formed para-nitroaniline (pNA) from the hydrolysis, which generates yellow coloration according to enzyme activity. The reaction was performed at 37°C for 1 h with or without the presence of various concentrations of each test compound. The absorbance (405 nm) was measured with a BioTek ELx800 microplate reader (Marshall Scientific, Hampton, NH, USA) [18].

The selected enzyme (2 nM) and substrate (0.5 mM) concentrations are typical of established kallikrein assay procedures [15,16] to allow for linear kinetics, as well as a suitable optical-density response without substrate saturation.

All experiments were performed in triplicate, and the assays were repeated three times (n = 3). The 100 % activity was determined with no inhibitor (enzyme-substrate) as a control reaction. Results were given as the mean ± SD. The IC_{50} values were determined using nonlinear regression (four-parameter logistic model) in GraphPad Prism 9.0 software (GraphPad Software, USA). Between-group differences were compared using one-way ANOVA followed by Tukey's post hoc test, and $p < 0.05$ indicated a statistically significant difference.

2.2. In silico methods.

This study employs an integrated in-silico workflow to evaluate the inhibitory efficacy of four ligands—three natural flavonoids (Fisetin, Morin, and Rutin) and the synthetic inhibitor sebetralstat—against human plasma kallikrein. DFT in Gaussian 16 (Rev. C.01) at the B3LYP/6-31G(d,p) level with an ultrafine integration grid was used to optimize the geometries.

SCF convergence was set to 1.0×10^{-8} Eh (SCF=VeryTight) and geometry convergence to Tight (max force 1.5×10^{-5} a.u.; RMS force 1.0×10^{-5} a.u.). Harmonic frequency analyses verified genuine minima (absent imaginary frequencies) and yielded thermochemical corrections at 298 K. When necessary, solvation was simulated with PCM (water, ε=78.4) employing the same convergence criteria. To find out how reactive an electron is, we used frontier orbital energies to find the HOMO–LUMO gaps (ΔE) [19]. Multiwfn generated electrostatic potential (ESP) maps, which were then visualized in VMD to examine charge distribution and possible electrostatic complementarity with the protein binding site [20,21]. To characterize weak binding interactions, non-covalent interaction (NCI) analysis was performed using NCIPLOT, focusing on hydrogen bonding and van der Waals forces via reduced density gradients [22].

We chose the plasma kallikrein structure (PDB ID: 7N7X, 1.9 Å resolution) because it shows a catalytically active conformation that was co-crystallized with an inhibitor. This gives us a reliable definition of the active site for docking. We used PyMOL and BIOVIA Discovery Studio [23-25] to look at binding energies and interaction profiles. We used AutoDock Vina 1.2.x to do the docking. Adding hydrogens, assigning Gasteiger charges, and removing crystallographic waters more than 5 Å from the binding site were all part of the protein preparation. Before docking, ligands were energy-minimized. The search box was 60 × 60 × 60 Å (1.0 Å grid spacing) and was centered on the catalytic pocket and S1 subsite. The Vina parameters were exhaustiveness = 16, num_modes = 20, and energy_range = 4 kcal·mol^{-1}. We confirmed the validity of the protocol by redocking the co-crystallized ligand. This reproduced the experimental pose with an RMSD of less than 2.0 Å, which is within the accepted range. This supports the reliability of the docking workflow.

Molecular dynamics (MD) simulations were conducted using GROMACS 2021.x with the protein force field and TIP3P water. Each protein–ligand complex was solvated in a triclinic dodecahedral box with 10 Å of padding, neutralized, and simulated in the presence of a NaCl concentration of 0.15 M. The energies were minimized to F_{max} < 1000 kJ·mol^{-1}·nm^{-1} by steepest descent. Equilibration was comprised of 500 ps in an NVT ensemble at 300 K (V-rescale thermostat, τ_T = 0.1 ps), and then a1 ns in an NPT ensemble at 1 bar (Parrinello–Rahman barostat, τ_P =2.0 ps; compressibility =4.5×10^{-5} bar^{-1}). Production runs were 100 ns each with a timestep of 2 fs, LINCS on hydrogen bonds, the Verlet cutoff scheme, Lennard-Jones cutoff at 10 Å, real-space Coulomb cutoff at 10 Å, and Particle Mesh Ewald (PME) for long-range electrostatics (FFT grid spacing ≈ 1.2 Å). The coordinates of structures were saved every 10 ps. Calculations were carried out using GROMACS tools and MDAnalysis. The first 20 ns were considered as equilibration after a stability assessment of temperatures and pressures, whereas the rest (80 ns) was for production. RMSD (Cα), per residue RMSF (Cα), radius of gyration (R_g), and solvent accessible surface area (SASA) were defined in a regular manner [26,27]. Stationarity was examined through visual inspection and block averaging of RMSD; plateaus within ~0.2 nm for ≥10 ns were considered as signs of stability.

ADMET profiling was conducted on the pharmacokinetic and toxicological properties—oral absorption, CYP450 metabolism, aqueous solubility, hERG inhibition, mutagenicity, and ecotoxicity—to provide an overall assessment of whether a compound would be a potent, selective plasma kallikrein inhibitor. Lipophilicity, drug-likeness, and permeability were predicted using SwissADME, while systemic ADMET results were provided by ADMETlab 2.0 and toxicity assessments by ProTox-II [28-32]. Unless otherwise specified, off-the-shelf models with platform-recommended thresholds were used.

2.3. Statistical analysis.

Data were obtained in triplicate from four unique experimental assays. GraphPad Prism 10.0 (GraphPad Software, Inc., San Diego, CA, USA) was utilized to assess the mean ± SEMs from the chromogenic enzymatic bioassays of plasma kallikrein using nonlinear regression. A one-way ANOVA followed by Dunnett's post hoc test was employed to analyze the data. Statistical significance for all comparisons was stated as $p < 0.05$.

3. Result and Discussion

3.1. Inhibitory effects of Fisetin, Morin, and Rutin on the activity of plasma kallikrein.

To evaluate the inhibitory effects of flavonoids on plasma kallikrein, three independent chromogenic assays were conducted in triplicate with a concentration range (1-1000 µM). Plasma kallikrein inhibitor, Sebetralstat, was utilized as a reference inhibitor (Figure 1A). The ability of plasma kallikrein to hydrolyze the chromogenic substrate S2302 was influenced by all three flavonoids significantly in a dose-dependent manner. The results of Fisetin and Morin compounds demonstrated superior plasma kallikrein enzyme inhibition compared to Rutin (Figure 1B). The statistical analysis of the data indicated that the IC_{50} values for the inhibitory effects of Fisetin, Morin, and Rutin on plasma kallikrein are 300.13 µM, 377.36 µM, and 566.04 µM, respectively. The efficacy of inhibitory Fisetin, Morin, and Rutin at 100% activity was evaluated using the control plasma kallikrein-protease enzyme value as a baseline comparison.

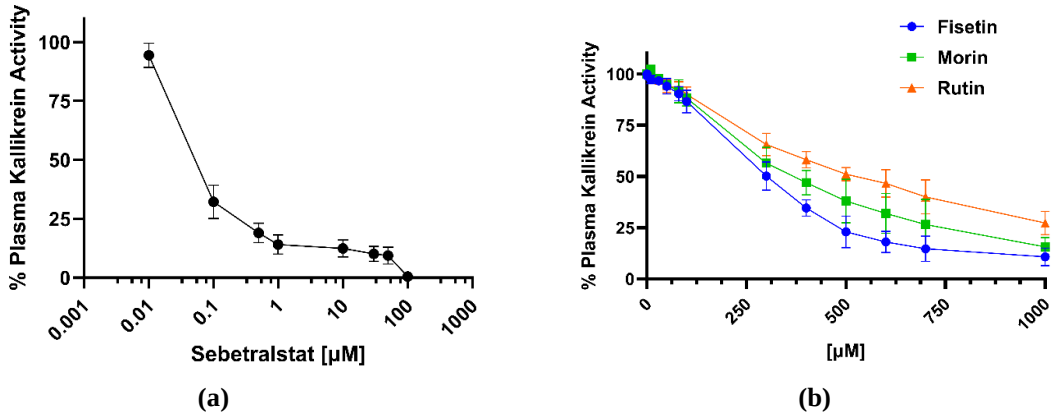

Figure 1. Inhibitory effects on human plasma kallikrein activity. **(a)** Effects of reference inhibitor Sebetralstat on plasma kallikrein activity. 2 nM plasma kallikrein enzyme and S2302 substrate (0.5 mM) were incubated in the absence or presence of increasing concentrations of Sebetralstat (0.1-100 µM); **(b)** Effect of flavonoids Fisetin, Morin, and Rutin on plasma kallikrein activity. 2 nM plasma kallikrein enzyme and S2302 substrate (0.5 mM) were incubated in the absence or presence of increasing concentrations of each flavonoid separately (1-1000 µM). For both panels, data are expressed as % mean ± S.E.M. for three independent triplicate experiments.

3.2. Analysis of the electronic properties of ligands by frontier molecular orbitals HOMO–LUMO.

The analysis of frontier molecular orbitals (HOMO–LUMO) constitutes a fundamental approach to predicting the electronic stability and potential reactivity of a ligand. The energy gap between the highest occupied molecular orbital (HOMO) and the lowest unoccupied molecular orbital (LUMO) allows for evaluating a compound's propensity to undergo charge transfer, participate in electronic interactions, or resist oxidation. In this section, we examine the electronic densities associated with the HOMO and LUMO orbitals as well as the energy

gaps (ΔE) of the ligands, Fisetin, Morin, Rutin, and Sebetralstat (Sebetralstat is a potent, oral, and selective plasma kallikrein inhibitor used for on-demand treatment of hereditary angioedema. It binds reversibly to the enzyme's catalytic domain, blocking bradykinin generation. In this study, it served as a benchmark for comparing the inhibitory potency of the tested flavonoids to better understand their electrochemical behavior in a biomolecular context. The visualization of the HOMO–LUMO orbitals and the corresponding energy gap values (ΔE) for these ligands are presented in Figure 2.

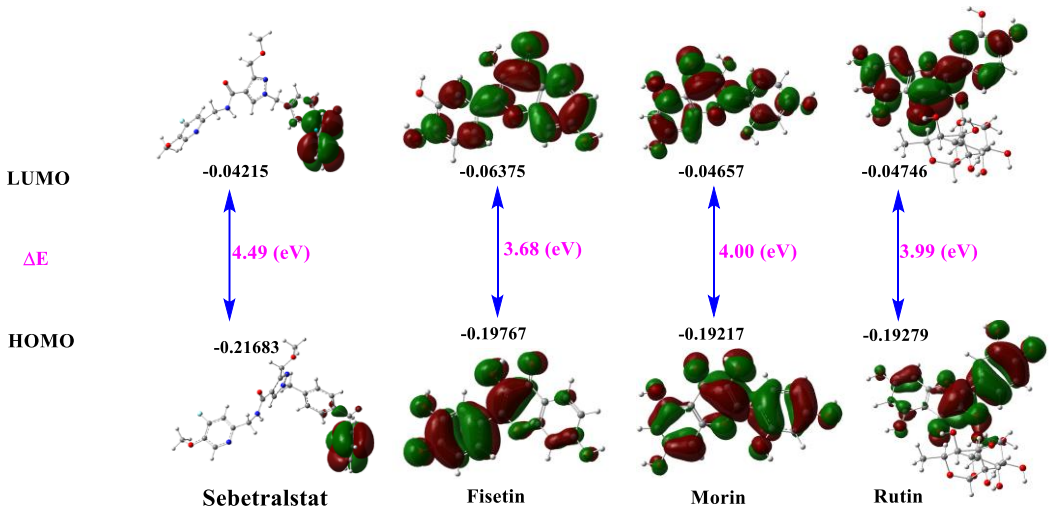

Figure 2. Visualization of the HOMO–LUMO orbitals and energy gaps (ΔE) of the ligands Sebetralstat, Fisetin, Morin, and Rutin.

Figure 2 shows the distribution of electronic densities of the frontier molecular orbitals HOMO (Highest Occupied Molecular Orbital) and LUMO (Lowest Unoccupied Molecular Orbital) for four ligands, Sebetralstat, Fisetin, Morin, and Rutin, as well as their corresponding energy gaps (ΔE, expressed in electronvolts). The analysis of the HOMO–LUMO orbitals is an essential step in characterizing the electronic reactivity and chemical stability of a compound. More specifically, the energy of the HOMO indicates a ligand's ability to donate electrons, while that of the LUMO reflects its ability to accept them. The energy gap ΔE (LUMO–HOMO) allows for the evaluation of the overall stability of the molecule: a high ΔE is generally associated with a chemically stable and less reactive molecule, while a low ΔE suggests greater reactivity.

According to the displayed values, Fisetin exhibits the lowest ΔE (3.68 eV), which reflects a higher chemical reactivity, potentially resulting in greater ease in establishing electrostatic interactions or electronic transitions. The other two ligands, Morin (ΔE = 4.00 eV) and Rutin (ΔE = 3.99 eV), occupy an intermediate position, with moderately stable electronic profiles but more reactive than Sebetralstat. The reference inhibitor Sebetralstat has the largest energy gap (ΔE = 4.49 eV), which indicates excellent electronic stability. This large difference between HOMO (–0.21683 eV) and LUMO (–0.04215 eV) confirms a low propensity for spontaneous electronic excitation, which is consistent with its structuring behavior observed in molecular dynamics analyses. In contrast, the three-dimensional visualization of the orbitals also shows notable differences in the localization of the electronic densities. In Sebetralstat, the orbitals are more widely distributed across the molecular skeleton, which may promote a more balanced interaction with the protein's active site. In contrast, in Fisetin, Morin, and Rutin, the HOMO and LUMO orbitals appear more localized, primarily on the substituted aromatic rings,

which can favor π–π interactions or localized charge transfers with certain residues of the binding site.

In summary, Fisetin, although more reactive, could prove more versatile in certain electronic interactions, while Morin and Rutin offer a good compromise between reactivity and stability compared to Sebetralstat, which showed the most electronically stable ligand.

The clinical relevance of plasma kallikrein inhibition extends beyond experimental enzymatic control. In hereditary angioedema (HAE), excessive activation of plasma kallikrein leads to uncontrolled bradykinin production and recurrent episodes of tissue edema. Current therapeutic strategies targeting kallikrein, such as ecallantide and lanadelumab, have demonstrated the efficacy of this enzyme as a validated drug target. Therefore, the identification of natural flavonoids with moderate but specific kallikrein inhibitory activity could offer alternative or adjunctive approaches for the prevention and management of bradykinin-mediated disorders, including HAE, diabetic macular edema, and inflammatory vascular pathologies.

3.3. NCI mapping of the ligands fisetin, Morin, Rutin, and sebetralstat.

The analysis of non-covalent interactions (NCI) constitutes a valuable approach to characterize the nature of the forces that stabilize or disrupt molecular complexes. By relying on the examination of electronic density gradients and the eigenvalues of the Hessian tensor, this method allows for the visual identification of attractive interactions (such as hydrogen bonds or π–π interactions), Van der Waals interactions, and steric repulsive interactions. In this section, we analyze the distribution of non-covalent interactions associated with the ligands Fisetin, Morin, Rutin, and Sebetralstat, with the aim of interpreting their spatial behavior and their ability to interact with a biological environment. The mapping of NCI interactions for these ligands is presented in Figure 3.

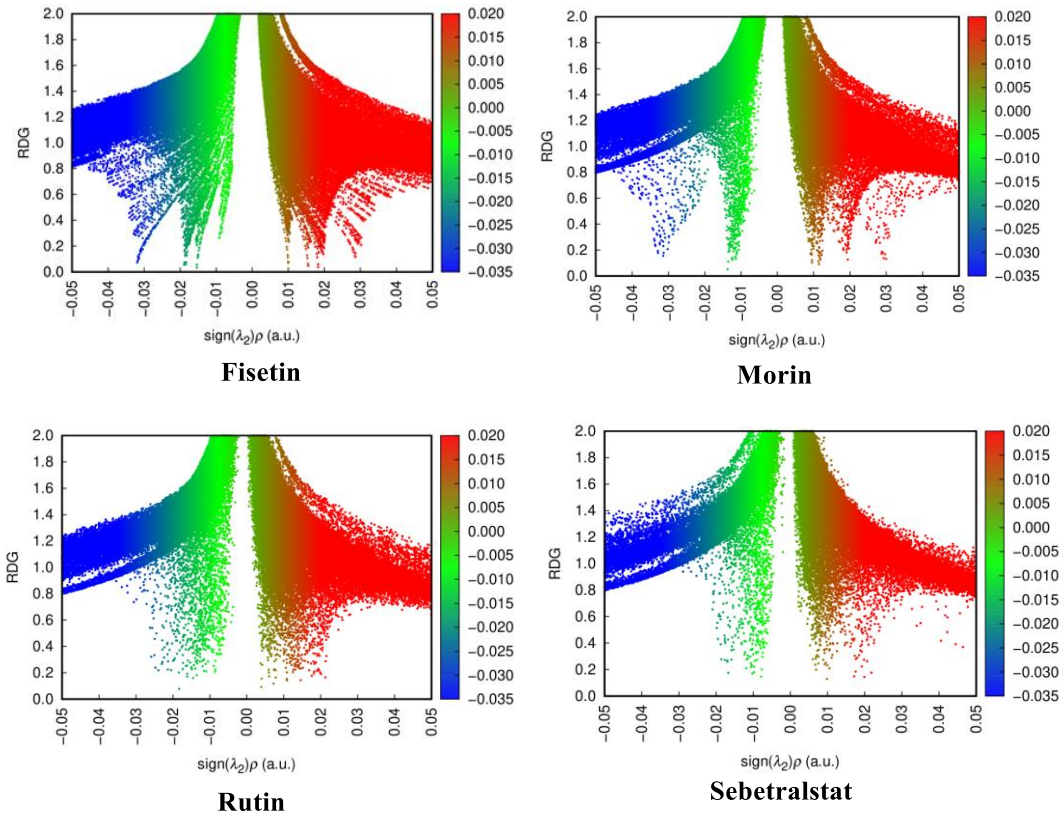

Figure 3. Non-covalent interaction (NCI) mapping for the ligands Fisetin, Morin, Rutin, and Sebetralstat.

Figure 3 shows the NCI (non-covalent interaction) representations of the four ligands Fisetin, Morin, Rutin, and Sebetralstat, illustrated through scatter plot-type diagrams (Representation of reduced electronic density vs the product of electronic density and density gradient). This method relies on the analysis of electronic density (ρ) and its gradient to detect, locate, and interpret non-covalent interactions in molecular systems. These representations allow for the differentiation of interaction types based on the value of the signed product $\lambda_2\rho$ (where λ_2 is an eigenvalue of the Hessian tensor of the density): negative values indicate attractive interactions (hydrogen bonds, electrostatic interactions), values close to zero correspond to Van der Waals-type interactions, and positive values indicate repulsive interactions (steric).

On the four graphs, the distribution of colored points according to the blue-green-red scale highlights distinct regions of interactions. First, the blue zones ($\lambda_2\rho < 0$) indicate strong attractive interactions, particularly hydrogen bonds or π-π stacking. These zones are clearly visible in Morin and Fisetin, indicating a significant ability to form stabilizing bonds. Second, the green regions ($\lambda_2\rho \approx 0$) are associated with Van der Waals-type interactions, which are weak but numerous and omnipresent in biological structures. All ligands exhibit a significant green component, indicating a favorable compatibility with a biomolecular environment. Finally, the red areas ($\lambda_2\rho > 0$) indicate the presence of repulsive effects (mainly due to steric hindrance between nearby groups). These interactions are slightly more pronounced in Rutin, probably due to its bulkier glycosylated structure compared to Sebetralstat, with less pronounced interactions.

These NCI representations thus allow for the comparison of the quality and nature of non-covalent interactions within the ligands. Morin and Fisetin exhibit a profile rich in attractive interactions, favorable for strong anchoring in a protein pocket. Rutin, although rich in interactions, seems penalized by greater steric hindrance, which could impair its ability to stabilize in restricted active sites. In comparison, Sebetralstat, despite moderate NCI activity, presents an optimal balance between weak interactions and limited repulsions. As a conclusion from the profiles of HOMO–LUMO, it was identified that Fisetin and Morin exhibited relatively smaller energy gaps (3.68 eV, 4.00 eV), indicative of their higher reactivity towards the catalytic residues of plasma kallikrein with pronounced charge-transfer ability. NCI mapping validated their dense hydrogen-bonding network and moderate steric hindrances, while Rutin exhibited stronger repulsion because of its bulking glycosidic part. These trends are similar to that of the docking, where Fisetin (–9.1 kcal mol^{-1}) and Morin (–8.6 kcal mol^{-1}) had stronger complexes than Rutin (–7.5 kcal mol^{-1}), which means ideal electronic flexibility and a moderate size are also in favor of efficient binding.

3.4. Docking study.

The study of the binding affinity between a target molecule and its ligands constitutes a crucial step in predicting the efficacy of a potential inhibitor. Molecular docking enables estimation of the binding free energy, reflecting the stability of the complex and the steric and electronic compatibility between the two partners. In this section, we compare the binding affinities of four ligands, Fisetin, Morin, Rutin, and Sebetralstat, in order to evaluate their interactive potential with human plasma kallikrein (7n7x). The free binding energy values (in kcal/mol), obtained through molecular docking simulation, are presented in Table 1, while the molecular interactions between the ligands Fisetin, Morin, Rutin, and Sebetralstat and human kallikrein (7n7x) are presented in Figure 4.

Table 1. Binding affinity energies (kcal/mol) obtained by molecular docking for the ligands Fisetin, Morin, Rutin, and Sebetralstat.

Ligand	Affinity (kcal/mol)
Fistin	-9.1
Morin	-8.6
Rutin	-7.5
Sebetralstat	-7.1

Table 1 summarizes the binding affinity values (expressed in kcal/mol) obtained from a molecular docking study, evaluating the interaction between a protein target (human kallikrein 7n7x) and four natural or semi-synthetic ligands: Fisetin, Morin, Rutin, and Sebetralstat. These values represent the free energy of ligand binding to the protein's active site; the more negative the energy, the more thermodynamically favorable the interaction. The analysis of the table shows that Fisetin has the highest binding affinity with a value of -9.1 kcal/mol, indicating a strong stability of the formed complex. Morin follows with a slightly lower affinity (–8.6 kcal/mol) but remains competitive. These two flavonoids, therefore, seem well adapted to the environment of the active site, probably due to their planar structure, the presence of hydroxyl groups, and their ability to form hydrogen bonds and π–π interactions. On the other hand, Rutin (–7.5 kcal/mol) and Sebetralstat (–7.1 kcal/mol) exhibit lower affinities; in the case of Rutin, the decrease could be related to its significant steric hindrance (glycosylation), which limits optimal access to the binding pocket. Regarding Sebetralstat, although it is known as a selective kallikrein inhibitor, this moderate affinity value could reflect a more specific but less energetic interaction in the docking model used, or result from an inhibition mechanism not solely based on binding free energy.

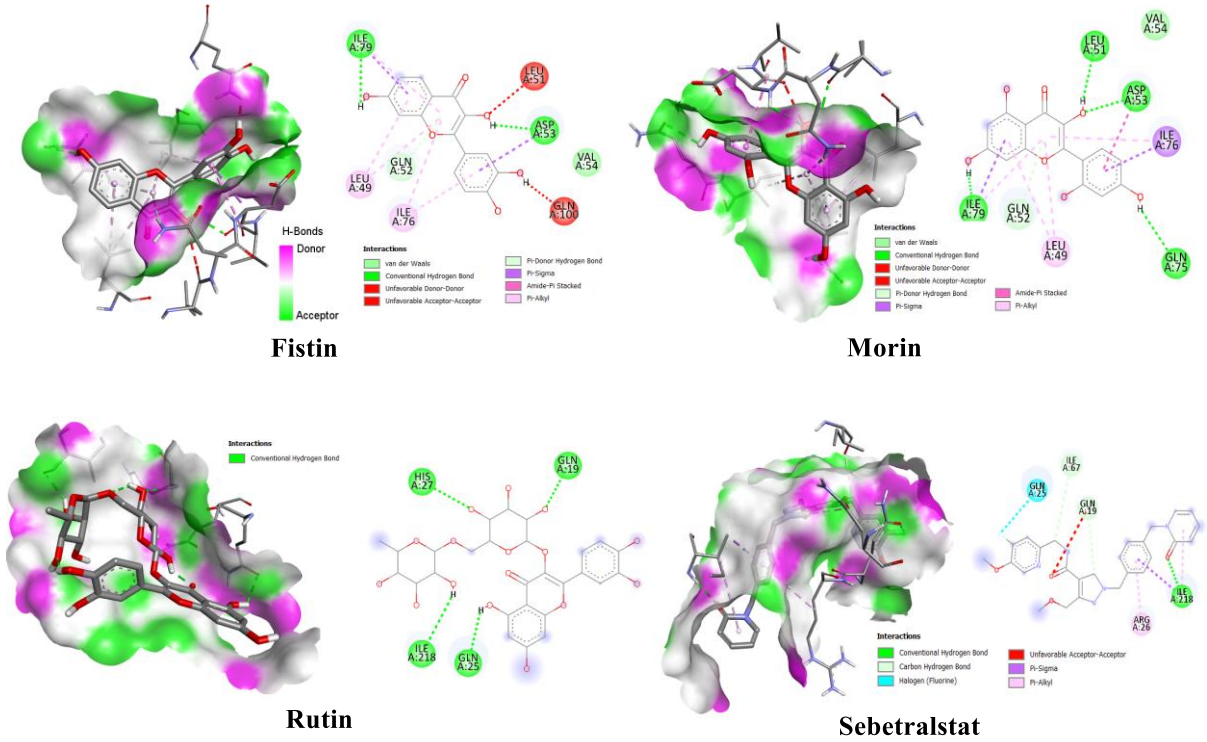

Figure 4. Visualization of the molecular interactions between the ligands Fisetin, Morin, Rutin, and Sebetralstat and human kallikrein (7n7x) obtained through molecular docking.

Figure 4 shows the molecular interactions established between four bioactive ligands (Fisetin, Morin, Rutin, and Sebetralstat) and human kallikrein (7n7x), as obtained by molecular docking. Each complex is visualized from a dual perspective: a 3D surface view highlighting the donor and acceptor regions of hydrogen bonds, and a 2D schematic view detailing the

protein residues involved in the interactions. The analysis reveals that the ligand fisetin establishes a dense network of conventional hydrogen bonds, particularly with the residues GLN A52 and GLN A79, as well as several hydrophobic interactions (π-donor, π-alkyl) with amino acids such as LEU A49, ILE A76, and VAL A54. This configuration suggests a stable and symmetrical anchoring in the active site. Morin exhibits a similar profile, with additional π–stacking and π–sigma interactions that reinforce the planar insertion of the ligand into the catalytic pocket. These observations confirm the good performance of Fisetin and Morin in terms of affinity and stability, as observed in the previous energetic analyses.

Rutin, despite several effective hydrogen bonds (notably with GLN A52, A79, and A138), appears to suffer from significant steric hindrance due to its bulky glycosylated structure. This constraint limits its penetration into the active site and concentrates its interactions at the periphery, which may explain its lower affinity. Finally, sebetralstat adopts a different anchoring mode, relying on a smaller number of hydrogen bonds but reinforced by targeted hydrophobic interactions (π-sigma, π-alkyl) and halogen-type bonds. Its behavior suggests a more specific inhibition mechanism, probably independent of the density of classical H bonds, but equally effective in terms of binding. Thus, this interactional mapping allows for a better understanding of differences in stability and affinity between the ligands and highlights the complementarities among the structural, energetic, and dynamic approaches used.

3.5. Elastic network and internal mechanical architecture of the protein 7n7x.

3.5.1. Conformation and dynamics of the 7n7x protein.

Molecular dynamics is a key approach to the study of proteins, reflecting their stability, potential interactions with other biologically significant molecules, and functional performance.

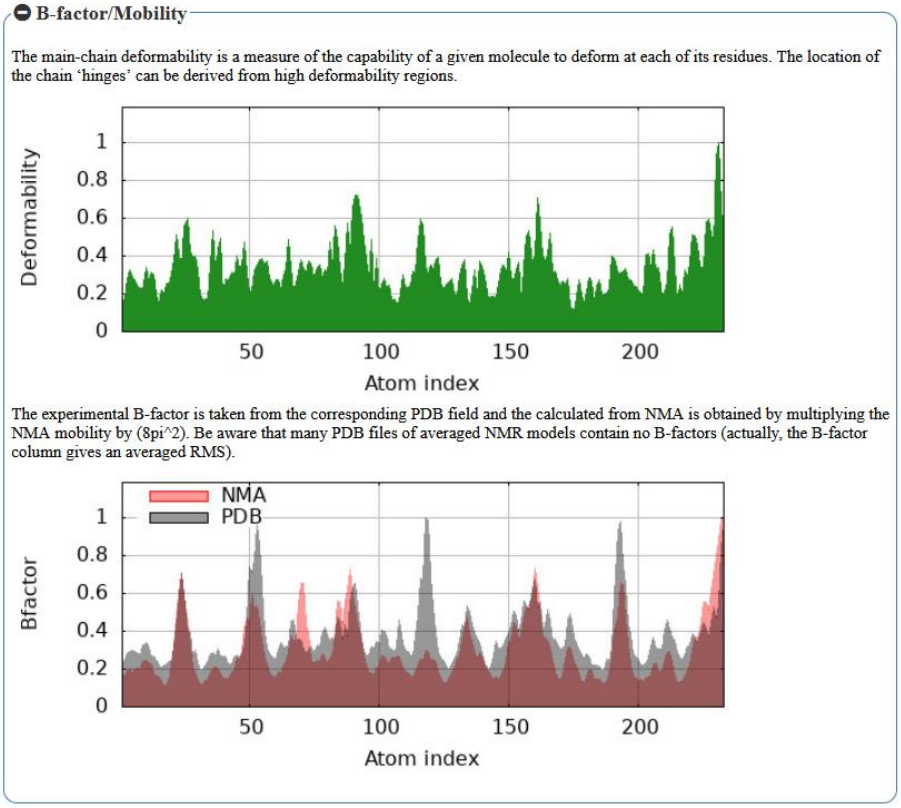

Figure 5. Evaluation of the structural flexibility of 7n7x: deformability profiles and experimental/theoretical B factors.

In addition to the static picture provided by crystallography, examination of conformational fluctuations informs us about the underlying mechanisms of enzymatic action and inhibition. In light of this, the current section of the manuscript is dedicated to investigating the interaction between human plasma kallikrein (7n7x), a serine protease that participates in the inflammatory and coagulation cascades, and the inhibitor Sebetralstat. Based on experimental data (factor B) and theoretical simulations (normal mode analysis), we identify the molecule's flexible and rigid regions to gain insight into the structural basis of its activity and inhibition. The major conclusions of this combined analysis are shown in Figure 5.

Figure 5 shows a more detailed structural analysis of the conformational flexibility of the human plasma kallikrein (7n7x) bound to the Sebetralstat selective inhibitor, which is a central serine protease of the contact cascade. This analysis is founded on two complementary approaches, which seek to describe the local dynamic properties of the molecule: residual deformability and the comparison of experimental with simulated B-factors. The residue deformability profile is plotted in the upper plot; it shows several sharp peaks close to indices ~25, 70, 100, 140, 190, and 220. These peaks represent protein regions with higher structural flexibility, usually located at loops, turns, or in the protein free end, which may have functional relevance such as ligand binding or conformational changes. In contrast, low deformability values are associated with stiffer regions held together by internal interactions and may act as structural cores of the protein.

The bottom graph compares the experimentally obtained B factors (B exp) (from X-ray crystallography data) with the B factors calculated from the normal mode analysis (NMA). The good general correlation between the two profiles confirms the adequacy of the theoretical dynamic model considered. The peaks common to the red (NMA) and gray (PDB) curves further support the assignment of flexible critical zones, whereas some differences seen in one point can be argued to be due to the intrinsic limitations of the harmonic model or to the crystallization conditions of the experiment. The cross-ratio of these two dynamic indicators, therefore, makes possible the reliable localization of the mobile, rigid, or disordered regions of the protein. They also enhance the exposure of the structure inhibition relationship of kallikrein 7n7x, particularly with respect to the molecular mechanism of inhibition by Sebetralstat, and lay out a platform for drug design based on the targeting of protein dynamically sensitive sites of this protease.

3.5.2. Modal analysis of overall flexibility of plasma kallikrein (7n7x).

The collective motion of a protein is crucial for us to catch the functional mode of the protein, especially the ligand binding/releasing or the enzymatic activation. Normal Mode Analysis (NMA) provides a way of modeling the fluctuations around the equilibrium conformation of a biomolecular structure and of characterizing the principal directions of deformation. This method offers useful information about the global flexibility as well as the intrinsic dynamics of the protein. Here, we analyze the eigenvalues of the first normal modes and their cumulative variance, hoping to find out the major dynamic features in the HM hPKa (7n7x). The Relative contribution of normal modes to the structural dynamics of kallikrein 7n7x is given in Figure 6.

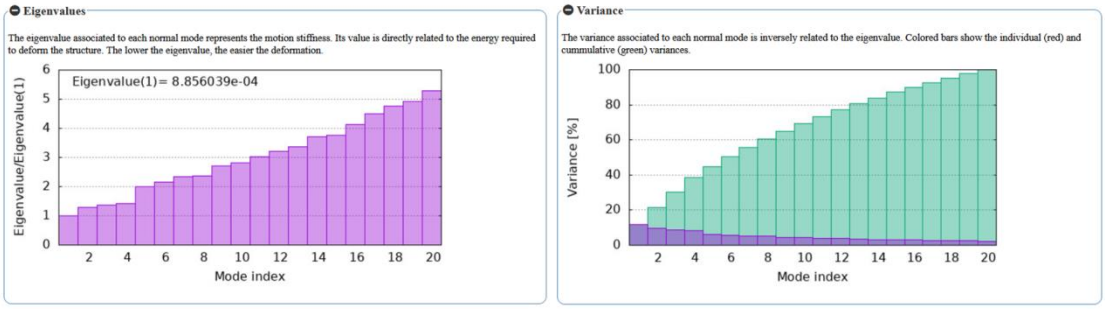

Figure 6. Relative contribution of normal modes to the structural dynamics of kallikrein 7n7x.

Figure 6 shows a representation of the intramolecular dynamics of human plasma kallikrein (7n7x), calculated using Normal Mode Analysis (NMA). It relies on the joint analysis of the eigenvalues (left plot) and of the cumulative variance (right plot), two key observables that provide insight into the collective fluctuations of the protein around its native state. The left panel shows the distribution of eigenvalues of the first 20 normal modes. Each of the eigenvalues appears to be scaling with the stiffness of the corresponding mode: the larger the scaling factor, the stiffer the mode is and presumably is involved in small and local structural changes; on the other hand, the smaller the scaling factor leading to smaller eigenvalues, the more flexible the mode could be and conceivably participate in larger and functional structural rearrangements. Therefore, the first mode, with a negligible eigenvalue (8.56×10^{-4}), indicates a large-scale collective motion that could be related to biologically relevant rearrangements, such as the opening of the active site, domain displacement, or structural adaptation promoted by the inhibitor Sebetralstat. The eigenvalues increase slightly with the mode index in a way that is associated with an increased rigidity, characteristic of more localized and less functional movements. The right graph, on the other hand, shows the percentage variance and displays the variance for an individual mode as well as the cumulative one. This discrepancy is inversely proportional to the eigenvalues: low-frequency modes, the most flexible ones, contribute a large value of the total structural flexibility. It is evident that the first five modes alone explain in excess of 60% of the cumulative variance, and that the first ten modes describe close to 80% of the total motion of the protein.

The above observation emphasizes the importance of these few modes of expressing biologically meaningful motions, with higher-order modes contributing little. This convergence of the data suggests that the majority of relevant noise is confined to a few collective modes, thereby supporting the application of dimension-reduction methods in dynamical studies. From a biological perspective, these results provide the means to identify beveling axes, structural hinges, or allosteric segments that may be recruited or mobilized upon enzymatic activation or inhibition. Low-frequency modes may also correspond to mechanisms of molecular recognition of the ligand, conformational adaptation to the ligand, or transmission of structural signals. In contrast, the stiffer modes make the positive contribution not only to the stability of the tertiary fold but to the integrity of the protein as a whole. Finally, our study illuminates the cooperative and organized Brownian nature of kallikrein 7n7x internal dynamics and could serve as a basis for determining functional modes, identifying dynamic targets for inhibition, or even rationally designing such ligands that modulate molecular flexibility.

3.5.3. Dynamic correlations among 7n7x residues according to the above analysis.

The internal motions of protein are determined not only by the motion of individual residues, but also by the collective correlations, which connect the distant parts of the sequences. The covariance map provides a useful tool to describe such dynamic relationships. It permits the determination of residues whose motions are correlated or anti-correlated, and thus complementary information can be obtained about activation, inhibition, or allosteric communications. This section focuses on the dynamic cross-correlations of the residues in human plasma kallikrein (7n7x), derived from the fluctuations calculated by NMA. In Figure 7, we provide the covariance map of the atomic fluctuations (or atomic displacement) on different residues of the human plasma kallikrein (7n7x).

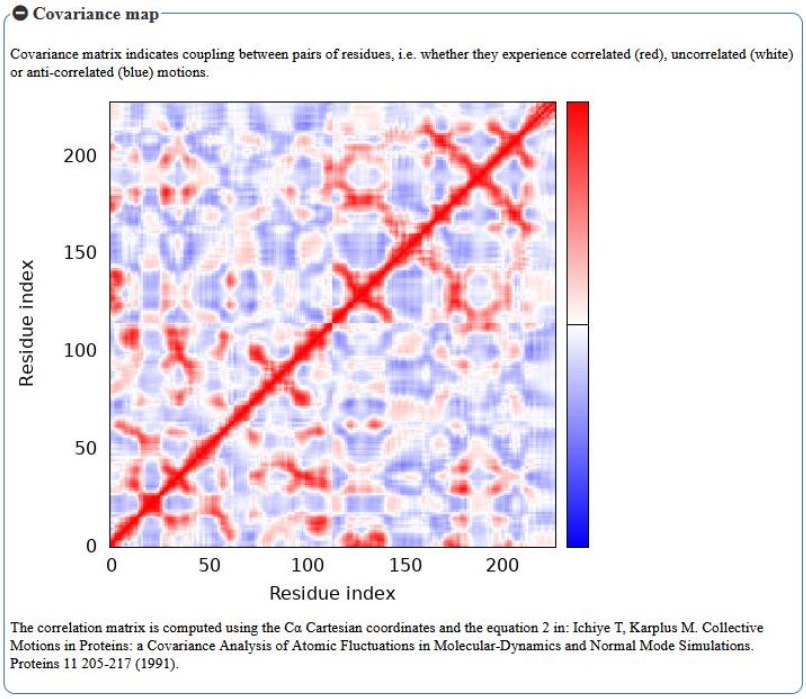

Figure 7. Covariance map of the 7n7x protein residues: correlations and anti-correlations of atomic movements.

Figure 7 is the covariance map of atomic displacements for different residues of human plasma kallikrein (7n7x) as modeled by NMA. This two-dimensional map is a symmetric n × n matrix, where each (i, j) element represents the correlation between the motions of the Cα atoms of residues i and j in the system. The colors indicate the strength and nature of the dynamic coupling, positive correlations (red) denote a similar type of motion (both residues move in the same direction), negative correlations (blue) mean the motion of one residue is opposite to that of the other, and no (or little) correlation is shown as white color. This depiction is a powerful approach to identifying dynamic connections that are not evident in the static three-dimensional structure.

First, we see a bright red diagonal, which, of course, is the maximum correlation of each residual with itself – something we expect and is trivial. In this vicinity, there appear a number of red/blue blocks, that is, dynamically coherent interfaces, as defined by sets of residues that move concertedly. Such blocks correspond to compact architectural elements, which may be catalytic domains, helical stretches, or collapsed β-sheets. A more interesting feature is that some colored patterns deviate from the main diagonal, and these correspond to long-range correlations between residues that lie far apart in primary sequence but near (or

functionally coupled) in three-dimensional space. This indicates the presence of intrinsic mechanical connections that enable the transmission of motions across the whole molecule.

The blue regions shown, especially those opposed to the red blocks, represent free opposing ends and correspond to hinge domains or pincers, where the protein parts either separate or approach each other. Such a dynamics is also typical for enzymes with an activation mechanism involving conformational closing or for allosteric proteins. In kallikrein 7n7x, these anticorrelated regions may not only be involved in the opening of the active site, but also in structural changes to accommodate the binding of the inhibitor ligand Sebetralstat.

These findings are even more important since kallikrein is a pivotal agent in the contact cascade, a pathophysiological process susceptible to both local and global conformational perturbation. Such a map also suggests the protein's organizational complexity: rather than serving as a stiff object, it is a network of cooperative and antagonistic motions, encoded with a dynamic logic that it uses to do its biological thing. It underlines the axes of structural communication across various regions of the molecule and has provided critical information for a deeper understanding of how a local event (such as binding to the inhibitor) might yield remote consequences through internal dynamics coupling. These results therefore add an important functional aspect to classical structural studies of the protein and to the role of its mechanical properties in its chemical and pharmacological functions.

3.5.4. Mechanical modelling of 7n7x using the elastic network model (ENM).

Knowledge of the protein's inner mechanical characteristics provides a critical handle on its cooperative motions and functional conformational switches. The three-dimensional conformation of a macromolecule can be represented by the Elastic Network Model (ENM) and simplified as a system of connected atoms connected by harmonic springs. This framework provides a method for inferring the relative stiffness of atomic contacts, and for visualizing regions of high or low mechanical stress. This methodology offers a solid basis to study the propagation of internal deformations, regarding activation mechanisms, allosteric modulation or enzymatic inhibition. Figure 8 Elastic network map of the 7n7x protein showing springs distribution and rigidity of the connections between atoms.

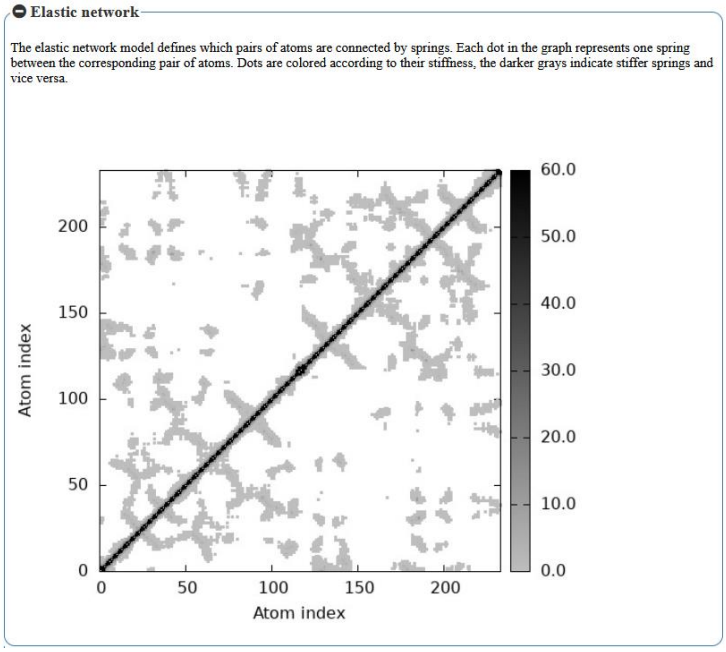

Figure 8. Distribution of internal mechanical forces of human kallikrein 7n7x modeled by ENM.

The ENM model of human plasma kallikrein (7n7x) that was used in Figure 8 is a serine protease. This model is based on a cartoon-like representation of the three-dimensional structure of the protein, where each atom (or Cα atom) forms a node and mechanical interactions between adjacent atoms are accounted for by harmonic springs. In the matrix, each matrix element can be interpreted as a spring between a pair of atoms, with springs of different rigidities indicated by the color scale (darker for stiffer interactions, i.e., stronger tension, and lighter for more flexible springs or the absence of a mechanical bond). The matrix main diagonal (strongly lined in black) shows highly strong interactions between nearest neighbors in the polypeptide chain due to an inner covalent bond. One also recognises, in the region around this diagonal, dark bricks related to the countrified motifs, such as α-helices or β-sheets that are regular enough to admit strong local constrained local interactions that stabilise the conformation.

The most striking features are the dark regions away from the diagonal, indicative of long-range mechanical linkages between atoms that are widely separated in sequence, but which are found in close proximity in the folded structure. These long-range springs are important contributors to the overall mechanical stability of the protein and allow mechanical signals to be transmitted through the network. This is particularly important for proteins that mediate allosteric mechanisms or conformational changes induced by ligand binding. On the contrary, unconnected areas of the structure, usually situated at the periphery of the molecule or belonging to flexible or floppy regions as loops, N- and C-terminal tails, correspond to the lighter/white regions of the matrix. By mapping the protein's implicit mechanical architecture, we can visualize which regions possess high internal rigidity, which are flexible, and identify possible pathways for mechanical transmission. To study the collective fluctuations of the molecule, modal analysis was carried out, but first, we need the normal mode calculation. For kallikrein 7n7x, with this sort of procedure, insight can be gained into the structural basis of its functional dynamics, as well as interesting prospects for investigating the mechanical effects that might be generated upon binding of the inhibitor Sebetralstat or upon targeted mutations. Therefore, this representation is more than a mere structural mapping; it provides an essential account of how structure, internal mechanics, and biological function in the protein are interrelated.

3.6. Molecular dynamics.

3.6.1. RMSD plot of human kallikrein complexes (7n7x).

Conformational stability of the complexes between the target protein and its ligands is a decision criterion to estimate the reliability and efficiency of molecular interaction. In this section, we discuss the root-mean-square deviation (RMSD) profiles of the protein human plasma kallikrein (7n7x) with the four ligands, namely, Fisetin, Morin, Rutin, and Sebetralastat. RMSD analysis enables comparison of the structural stability of each complex as it evolves during the 100-ns MD simulation, thereby identifying the most stable systems and those more likely to maintain the protein's functional conformation. Figure 9 shows the time traces of the RMSD profiles for the tested complexes.

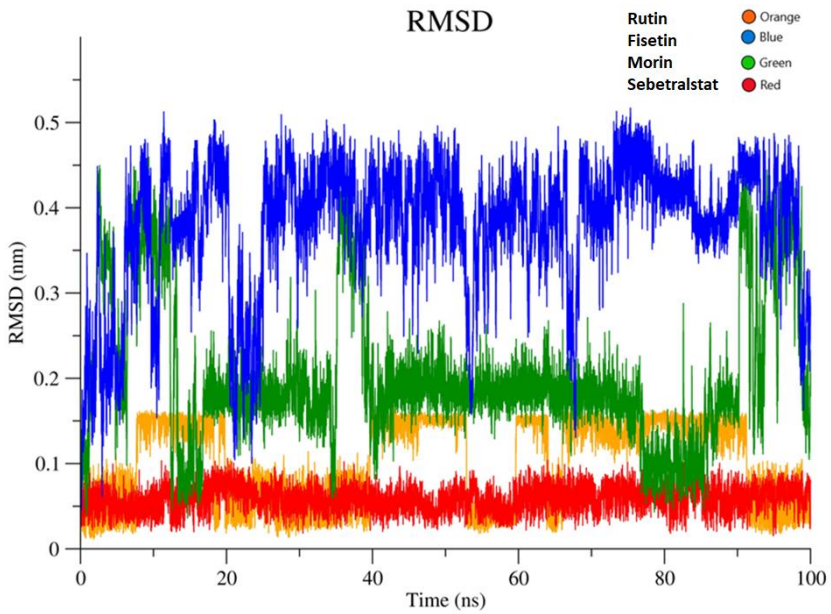

Figure 9. RMSD profiles of the 7n7x complexes with Fisetin, Morin, Rutin, and Sebetralstat over 100 ns of simulation

Figure 9 shows the root-mean-square deviation (RMSD) profiles obtained from 100-nanosecond molecular dynamics simulations of the 7n7x protein (the active form of human plasma kallikrein) complexed with four different ligands: Fisetin, Morin, Rutin, and Sebetralstat. The RMSD allows for the evaluation of the overall structural variations of the protein relative to its initial conformation over time and serves as an indicator of the conformational stability of the complex. A low and stable RMSD indicates good structural stability of the system, while significant fluctuations suggest structural readjustments or disorganizations. Analysis of the curves clearly indicates substantial differences between these four complexes. The Fisetin-7n7x complex, colored in blue, exhibits higher RMSD values (between 0.35 and 0.5 nm) and never fully reaches stability during the simulation. This behavior reflects a low overall structural stability, indicating that Fisetin does not promote stable protein structuring during binding and may also perturb the native conformation of 7n7x. In contrast, the Morin-7n7x complex, in green, shows an intermediate RMSD profile, with its values oscillating mainly between 0.2 and 0.3 nm, and some transient peaks. This dynamic suggests that Morin is less of an extreme anchor than Fisetin, as a little more protein would be held in the complex, but not in a very stable form: the protein would retain some flexibility, which may be advantageous for some activities but is also risky for long-lasting inhibition.

The contours of the Rutin–7n7x complex (orange) depict low and regular RMSD values, ~0.1–0.15 nm, with a few local peak values. This profile indicates overall acceptable global stability with potential local perturbations, as already suggested by previously reported RMSF (residue fluctuations) analyses. The last one showed enhanced flexibility in some loops, especially in the region of residue 1800, which is probably involved when it approaches Rutin. Thirdly, the Sebetralstat-7n7x complex (red), representing a single inhibitor, yields the best results: the RMSD curve remains almost constant, oscillating around 0.08–0.1 nm over the simulation. This has value as a rigidifying and structuring interaction, conferring on the protein the rigidity conducive to efficient, selective inhibition without addressing its 3-D structure. The RMSD profiles indicate moderate stabilizing behaviour; however, further analysis (RMSF, hydrogen interactions, binding energy) is needed to confirm their inhibitory power.

3.6.2. Atomic fluctuations RMSF of 7n7x–ligand complexes.

Calculating RMSF (root mean square fluctuations) provides information on the local flexibility of residues in the protein during the course of a molecular dynamics simulation. Unlike the RMSD, which quantifies overall structural deviations, the RMSF reveals regions, such as loops, termini, or exposed segments, that are highly mobile. For this portion, the RMSF in Human kallikrein (7n7x) with the four ligands Rutin, Fisetin, Morin, and Sebetralstat are compared to determine the effect of each molecule on the local stability of the protein. The curves related to the evolutionary curve of the RMSF calculated over 100 ns of dynamics are shown in Figure 10.

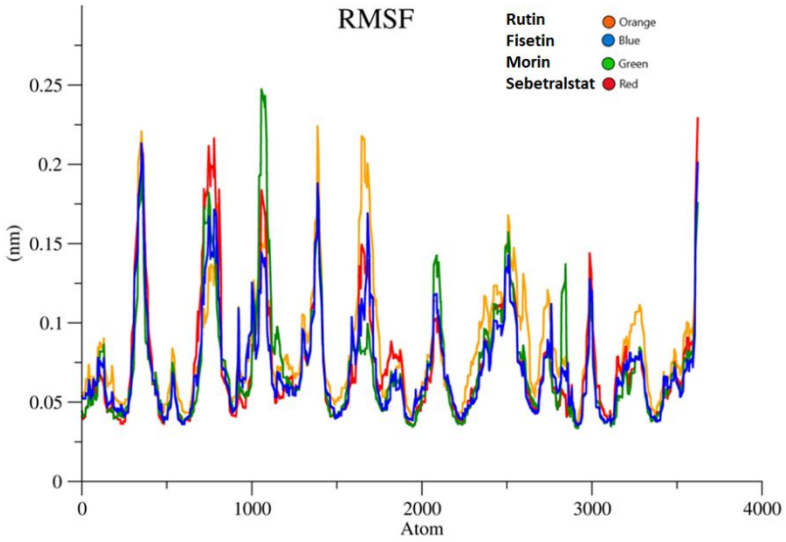

Figure 10. The RMSF profiles of the 7n7x protein in complex with Rutin, Fisetin, Morin, and Sebetralstat along 100 ns of simulation.

Figure 10 shows the root mean square fluctuation profiles of human plasma kallikrein (7n7x) with respect to atomic coordinates of whole protein (aas) in complex with four ligands: Sebetralstat (red), Morin (green), Fisetin (blue), and Rutin (orange). RMSF provides an estimate of the local flexibility of each atom with respect to its average location during the MD. It can therefore be considered a good measure of local flexibility in the protein structure, helping pinpoint the more dynamically unstable regions, such as loops, termini, or disordered regions. Overall, the profiles show a nice stability of the complexes with RMSF values being less than 0.25 nm over most of the chain. Yet, various peaks of the fluctuation function can be seen, indicating regions with enhanced flexibility. Among the tested ligands, Rutin (orange) shows the strongest fluctuations, especially around atomic positions 500, 1000, and 2500, possibly leading to local perturbations in the protein shape. In contrast, the Sebetralstat complex (red) exhibits the lowest RMSF values and peaks, and shows clear stabilization at the atomic level. Morin (green) and Fisetin (blue) have intermediate profiles, providing a gradual suppression of fluctuations in certain regions. These outcomes are fully consistent with the RMSD calculation, which confirms that Rutin, despite its binding, appears to induce local structural perturbations. Therefore, the radius of gyration can also provide insight into the influence of ligands on the protein's internal dynamics by determining regions susceptible to conformational perturbation upon ligand binding.

3.6.3. The 7n7x–ligand complexes were analyzed by the radius of gyration in order to evaluate structural compactness.

The radius of gyration (Rg) is a basic characteristic to estimate the 3D compactness of a protein in molecular dynamics simulations. It informs about the stability of the folding of the overall structure and enables one to monitor potential relaxations or perturbations triggered by ligand binding. In this work, we studied the time evolution of the radius of gyration of the human kallikrein (7n7x) complexed with the four proposed ligands Sebetralstat, Morin, Fisetin, and Rutin, to assess their relative effects on the structural stability of this complex structure. The radius of gyration during the evolution of the radius of gyration for 100 nanoseconds of simulation is shown in Figure 11.

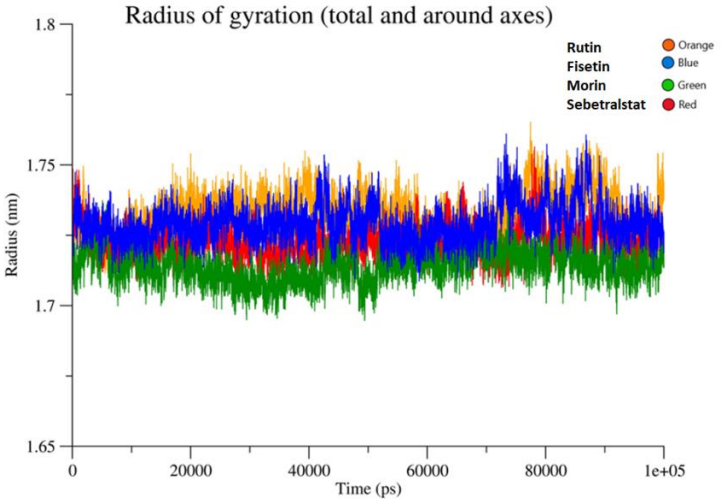

Figure 11. Evolution of the radius of gyration of the 7n7x protein complexed with Rutin, Fisetin, Morin, and Sebetralstat during 100 ns of simulation.

Figure 11 shows the evolution of the radius of gyration (Rg) of human plasma kallikrein (7n7x) during 100-nanosecond molecular dynamics simulations, in the presence of four potential ligands: Sebetralstat (red), Morin (green), Fisetin (blue), and Rutin (orange). The radius of gyration is a structural parameter that reflects the overall compactness of a protein by measuring the average distance of atoms from their center of mass. A low, constant Rg indicates a compact, stable structure, while an increase or significant fluctuations may signal loosening or structural instability. Among the analyzed complexes, the one formed with Sebetralastat shows the most stable and compact behavior, with a very regular Rg around 1.70 nm and low fluctuations throughout the simulation.

This profile also attests a good stabilization of the protein by the ligand, supporting Sebetralastat's structuring function. Likewise, the complex with Morin exhibits a small increment of compacity (slightly less Rg), which reinforces a good stabilizing interaction, although a bit more flexible. On the other hand, the Fisetin complex shows a higher Rg (1.72-1.74 nm) and larger fluctuations, consistent with a more relaxed, less confined structure that remains globally stable. At last, complex with Rutin is displaying max Rg values (1.74-1.76 nm) along with continuous fluctuations, which suggests a possibility of structural relaxation.

This behavior suggests that Rutin, despite having a binding affinity, could locally disrupt the protein's conformation and compromise its long-term stability. Thus, analysis of the radius of gyration allows us to differentiate the structural effects of the ligands tested on 7n7x, highlighting the superior stabilizing effect of Morin among the three flavonoids, while Fisetin

and Rutin appear less effective in maintaining the three-dimensional integrity of the protein compared to Sebetralstat.

3.6.4. Assessment of the structural compactness of the 7n7x–ligand complexes from the solvent accessible surface.

It is a potential parameter for assessing the extent of compaction or expansion of the protein during the molecular dynamics simulation. It lets us determine how much the shape remains folded or whether it is conformationally relaxed, depending on the interactions it forms with diverse ligands. Here, the SASA profiles of the human kallikrein (7n7x) with four ligands, Rutin, Fisetin, Morin, and Sebetralstat, are compared in order to assess how each molecule affects the exposure of the protein surface to the solvent. The time development of the solvent-exposed surface over 100 ns is shown in Figure 12.

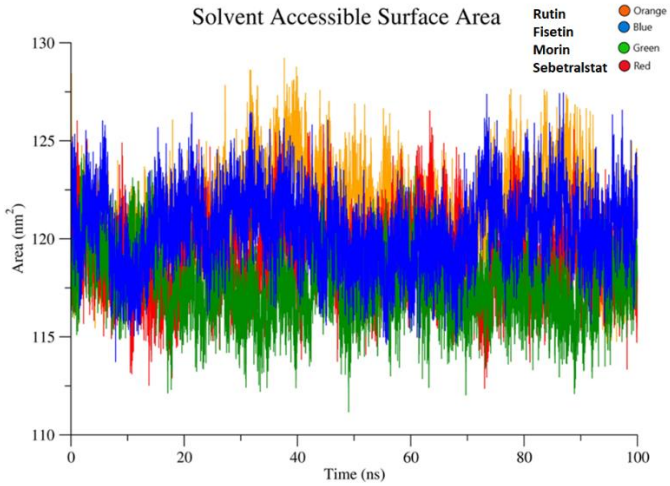

Figure 12. Evolution of the solvent accessible surface area (SASA) of the 7n7x protein complexed with Rutin, Fisetin, Morin, and Sebetralstat over 100 ns of simulation.

Figure 12 illustrates the evolution of the solvent-accessible surface area (SASA) of human plasma kallikrein (7n7x) during a 100-nanosecond molecular dynamics simulation, interacting with four different ligands: Rutin (orange), Fisetin (blue), Morin (green), and Sebetralstat (red). The SASA estimates the surface area of the protein in contact with the solvent and serves as an indirect indicator of the protein's compactness or openness. A lower SASA value is generally associated with a compact and well-folded structure, while a higher value indicates a more relaxed state, potentially less stable.

From the analysis of the curves, it is evident that the Rutin and Fisetin complexes have the highest SASA values, often lying between 120 and 127 nm². This suggests a more exposed protein surface to the solvent, indicating that these ligands do not cause a high degree of tightening of the protein and may even induce a partial opening of the conformation.

On the other hand, complexes with Morin and especially with Sebetralstat, present smaller values between 113-117 nm², corresponding to more compact structures; this trend is particularly evident for Sebetralstat, whose curve is not so much low as regular, which adds consistency to the structuring and stabilizing function already detected in RMSD, RMSF, and Rg analyses. Since fluctuations are inherent in such a simulation, the average surface deviations between the ligands lead us to conclude that Fisetin and Rutin seem to favour more open states, possibly associated with local dynamical perturbations, or with a weaker stabilising affinity

towards the binding site compared to Sebetralstat, which keeps kallikrein in a compact, stable configuration.

3.6.5. Hydrogen bonding network for human kallikrein 7n7x and its ligands.

Hydrogen bonds are important in stabilizing and specifically recognizing protein-ligand complexes. They help position the ligand appropriately within the binding cavity and have a remarkable impact on the interaction energy and the dynamics of the complex. The analysis of the development of the quantity of hydrogen bonds between human kallikrein (7n7x) and four ligands, Rutin, Fisetin, Morin, and Sebetralstat, is performed in this section to evaluate the dynamic and persistent characteristics of the interactions during the MD simulations. In Figure 13, we show the time dependence of the number of hydrogen bonds over 100 ns of simulation.

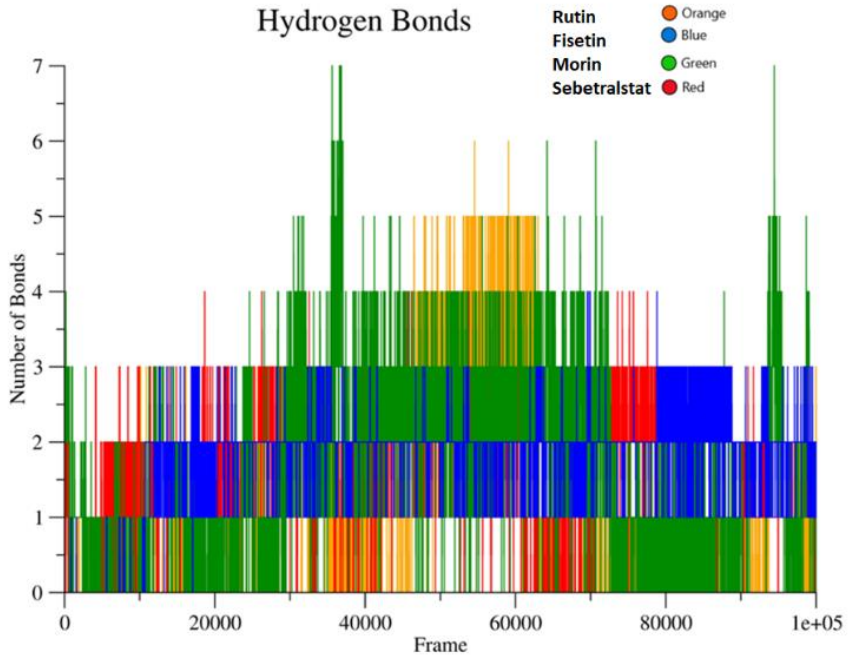

Figure 13. The Number of Hydrogen bonds developed between the protein 7n7x and Rutin, Fisetin, Morin, and Sebetralstat during 100ns of MD simulation

Temporal evolution of the number of hydrogen bonds formed between the 4 ligands: Rutin (orange), Fisetin (blue), Morin (green), and Sebetralstat(red), and the 7n7x protein is shown from 0 to 100,000 simulation steps (0 to 100 ns) in Figure 13. The quantity and type of hydrogen bonds are among the most important manifestations of the quality of molecular interactions between drugs and targets 1. They play key roles in selective recognition, conformational stability, and binding affinity of protein-ligand complexes. A stable and properly oriented hydrogen bond can also increase the stability of ligand anchoring in the active site, reduce local fluctuations, and enhance the compound's inhibitory potency.

The examination of the profiles shows that the 7n7x–Morin complex (green curve) is clearly distinguished by the formation of a dense, persistent network of hydrogen bonds, often involving 3-6 simultaneous bonds, particularly between 30,000 and 80,000 frames. This behavior reflects a multivalent, highly stabilizing interaction, likely related to the presence of multiple hydroxyl groups on the Morin molecule, optimally oriented toward the residues of the active site. This type of anchoring favors a durable occupation of the ligand, with spatial locking that stabilizes the target protein's conformation.

In contrast, Fisetin (blue) forms, on average, 1 to 3 hydrogen bonds, with a more regular but less intense distribution, suggesting a moderate but constant interaction, sufficient to maintain the complex without an enhanced stabilization effect.

Sebetralstat (red) shows a particular profile: hydrogen bonds are few and sporadic, most often fewer than 2, and often absent over long portions of the simulation. This suggests that its anchoring mode relies primarily on non-covalent interactions, particularly hydrophobic, ionic, and van der Waals interactions, consistent with its specific chemical structure and the high level of compaction observed in other parameters (Rg, SASA). Rutin (orange), on the other hand, forms a moderate number of hydrogen bonds at the beginning of the simulation, with a gradual increase around 40,000–60,000 frames, followed by a decrease towards the end, indicating a more unstable or transient interaction, possibly related to a reorientation or migration of the ligand within the binding pocket.

These findings indicate that all ligands do not stabilize the protein in an equivalent manner. Morin has the largest, longest, and most dense hydrogen network, even though it has a small number of hydrogen bonds. Sebetralstat, despite this, is able to be effective in other structural elements (conformational stability, packing, small RMSD), which indicates a more likely hydrophobic or steric binding mode. The fact that those different profiles are complementary to each other is indicative that a ligand can stabilize a protein in different ways and that, therefore, the assessment of inhibitory potential should not only be restricted to counting hydrogen bonds but also to how well they integrate into the entire set of dynamic descriptors. In conclusion, the structural properties determining dynamic stability were summarized in Terms of the key parameters over 100 ns. Sebetralstat had the minimum RMSD (0.09 nm) and Rg value of 1.70 nm, indicating a more compact profile. Morin has an intermediate RMSD (0.28 nm), whereas Fisetin and Rutin showed high RMSD and SASA values, indicating local flexibility and partial unfolding. The average number of hydrogen bonds (Sebetralstat = 2, Morin = 4, Fisetin = 2, and Rutin = 1) hints at these stability trends. Overall, Morin appears as the most compact flavonoid–protein complex, like the reference inhibitor.

3.7. ADMET investigation.

The analysis of pharmacokinetic properties (ADME) is an essential step in the screening of bioactive molecules, particularly for predicting their behavior in vivo before experimental phases. The in silico evaluation allows for the anticipation of intestinal absorption, tissue distribution, metabolic interactions (notably enzymatic), as well as solubility and permeability parameters. In this section, we compare the ADME profiles of the four studied ligands, Fisetin, Morin, Rutin, and Sebetralstat in order to identify those with the best biopharmaceutical properties. The results for the pharmacokinetic parameters are presented in Table 2, while the predictive data on the toxicity of these ligands are presented in Table 3.

Table 2. In silico evaluation of the pharmacokinetic properties (ADME) of the ligands Fisetin, Morin, Rutin, and Sebetralstat.

ID	Fisitin	Morin	Rutin	Sebetralstat
BBB	0.566596	0.286931	0.0296906	0.0182063
Buffer_solubility_mg_L	139,748	77,0733	112,347	976,244
Caco2	18,49	20,289	8,77131	40,1704
CYP_2C19_inhibition	Inhibitor	Inhibitor	Inhibitor	Non
CYP_2C9_inhibition	Inhibitor	Inhibitor	Inhibitor	Inhibitor
CYP_2D6_inhibition	Non	Non	Non	Non
CYP_2D6_substrate	Non	Non	Non	Non

ID	Fisitin	Morin	Rutin	Sebetralstat
CYP_3A4_inhibition	Inhibitor	Inhibitor	Inhibitor	Non
CYP_3A4_substrate	Weakly	Weakly	Weakly	Substrate
HIA	80,773991	66,789451	3,159758	96,595391
MDCK	247,028	31,202	0.0517434	0.187134
Pgp_inhibition	Non	Non	Non	Inhibitor
Plasma_Protein_Binding	94,038813	97,582151	61,702822	88,995587
Pure_water_solubility_mg_L	365,609	1553,58	443,354	4,39135
Skin_Permeability	-4,12767	-4,25107	-4,47234	-3,46333
SKlogD_value	2,06961	1,54249	-0,66458	3,20998
SKlogP_value	2,06961	1,54249	-0,66458	3,20998
SKlogS_buffer	-3,31145	-3,59351	-3,72508	-2,70111
SKlogS_pure	-2,89378	-2,28908	-3,12889	-5,04807

Table 2 presents the results of the in silico evaluation of the pharmacokinetic (ADME) properties of the four studied ligands: Sebetralstat, Rutin, Fisetin, and Morin. These parameters allow for the anticipation of the behavior of molecules in the body, particularly in terms of absorption, distribution, metabolism, and excretion. The data analysis shows that Fisetin and Sebetralstat have the best intestinal absorption capacities, with HIA rates of 80.77% and 96.59%, respectively, while Rutin has a very low absorption (3.16%). In terms of cellular permeability, Sebetralastat shows the best performance on the Caco-2 model (40.17) and good solubility in the buffer (976 mg/L), but very limited solubility in pure water (4.39 mg/L), which could pose a problem in terms of bioavailability. Fisetin and Rutin, on the other hand, exhibit good solubilities in pure water, which promotes their dispersion, but have more moderate permeability.

Regarding the blood-brain barrier (BBB), only Fisetin shows a significant permeability (0.57), suggesting possible activity in the central nervous system. All the compounds show low skin permeability, which limits their use in transdermal administration. The analysis of enzymatic interactions reveals that Sebetralstat is the only ligand that does not inhibit the cytochromes. CYP2C19 and CYP3A4, which offer a significant advantage in terms of safety and drug compatibility; on the other hand, Fisetin, Morin, and Rutin are all inhibitors of these enzymes, which can lead to undesirable drug interactions. None of the ligands are substrates or inhibitors of CYP2D6.

From a distribution perspective, the four ligands exhibit strong binding to plasma proteins (>88%), with Morin exhibiting the highest binding (> 97.58%), which may limit their free active fraction. Finally, the lipophilic parameters (logP/logD) reveal that Sebetralstat is the most lipophilic compound (logP = 3.21), which favors membrane permeability but limits aqueous solubility. Rutin, on the other hand, is very hydrophilic (logP = –0.66), which explains its low permeability. In summary, Fisetin presents a favorable profile, while Morin remains competitive but more protein-bound. Rutin, on the other hand, shows significant limitations in absorption and permeability, likely due to steric hindrance. Sebetralstat exhibited combining high absorption, good permeability, and low enzymatic interaction, despite limited aqueous solubility.

Table 3. Predictive evaluation of the toxicity of Fisetin, Morin, Rutin, and sebetralstat.

ID	Fisitin	Morin	Rutin	Sebetralstat
algae_at	0.0399242	0.0303054	0.00389677	0.0197431
Ames_test	mutagen	mutagen	Mutagen	mutagen
Carcino_Mouse	negative	negative	Negative	positive
Carcino_Rat	negative	positive	Negative	positive
daphnia_at	0.173085	0.17818	1,1518	0.0603247
hERG_inhibition	medium_risk	medium_risk	Ambiguous	medium_risk
medaka_at	0.0481279	0.052536	2,54783	0.00860382

ID	Fisitin	Morin	Rutin	Sebetralstat
minnow_at	0.0313091	0.0323288	1,73292	0.0277708
TA100_10RLI	negative	negative	Negative	negative
TA100_NA	negative	negative	Negative	positive
TA1535_10RLI	negative	negative	Negative	negative
TA1535_NA	negative	negative	Negative	negative

Table 3 presents an in silico predictive evaluation of the toxicity of the four studied ligands, Fisetin, Morin, Rutin, and Sebetralstat, based on several biological and environmental indicators. All the compounds are identified as mutagens in the Ames test, suggesting a potential genotoxic risk. However, these results should be interpreted with caution, as in silico predictions can vary depending on experimental conditions and require in vitro validation. Regarding carcinogenicity, Fisetin and Rutin present a reassuring profile with negative predictions in both mice and rats, while Morin is predicted to be positive only in rats. Sebetralastat, on the other hand, shows positive results in species, indicating a higher carcinogenic risk and justifying further toxicological studies.

In terms of cardiotoxicity, evaluated via predicted hERG channel inhibition, Fisetin, Morin, and Sebetralstat are classified as presenting a moderate risk, while the result for Rutin is deemed ambiguous, indicating either model uncertainty or sensitivity to the molecular context. The targeted mutagenicity tests (TA100 and TA1535) are overall negative for all ligands, except for Sebetralstat, which shows a positive result in the TA100_NA test, reinforcing the warning signal regarding its potential mutagenicity under specific conditions.

Regarding aquatic ecotoxicity, the predicted toxicity values for organisms such as Daphnia, Medaka, and Minnow indicate that Rutin is the most concerning from an environmental perspective, with high values across all species. Conversely, Fisetin, Morin, and Sebetralstat exhibit much lower toxicity levels, particularly Sebetralstat, which shows the lowest values for Medaka (0.0086) and Daphnia (0.0603), indicating better ecological compatibility. In summary, Fisetin and Morin exhibit relatively safe toxicological profiles despite their predicted mutagenicity, while Sebetralstat combines low environmental toxicity with a higher carcinogenic risk. Rutin, on the other hand, is both mutagenic and ecotoxic, which greatly limits its potential as a therapeutic candidate. From the ADMET investigation, Fisetin is the only compound with good absorption (HIA ≈ 81%) and moderate plasma protein binding (94%), among all compounds. Morin exhibits a somewhat diminished absorption but has superior stability and reduced estimated toxicity. On the other hand, Rutin has low permeability and high ecotoxicity, thereby limiting its pharmacological applications. These findings support Fisetin and Morin as hit scaffolds, whereas Rutin's highly polarized surface area accounts for its poor cell uptake and instability in solutions. In addition, the combined analysis of in vitro and in silico data demonstrates coherence between the analytical levels. The lower IC_{50} concentrations of Fisetin (300.13 µM) and Morin (377.36 µM) are consistent with their high docking affinities (-9.1and -8.6 Kcal mol^{-1}) and stable MD profiles, confirming the reliability of computational studies. In contrast, the lower activity of Rutin agrees with its poor ADMET and dynamic properties. Together, these corroborative results reinforce the robustness of molecular modeling for screening potential plasma-kallikrein inhibitors before cellular or in vivo validation.

4. Conclusion

The inhibitory effects of three natural flavonoids, Fisetin, Morin, and Rutin, on human plasma kallikrein were investigated using a combined in vitro enzymatic assay and in silico modeling approach, with Sebetralstat as the reference inhibitor. The in vitro results correlated well with a concentration-dependent inhibition. Fisetin and Morin have moderate inhibitory activity (IC_{50} of 300.13 µM and 377.36 µM), and Rutin was less active than those two compounds.

These in vitro findings were further validated by computational studies, in which Fisetin and Morin showed high binding affinities, stable protein–ligand complexes throughout molecular dynamics simulations, and optimal ADMET profiles; in contrast, Rutin exhibited low permeability and local structural perturbations. While this study makes a successful in vitro and in silico combination, it is restricted to a single assay model, heavily dependent on computational predictions, and tests only three flavonoids. As such, further general analog screening and testing are deserved.

Taken together, these findings suggest that Fisetin and Morin are potential natural scaffolds for plasma kallikrein inhibitors, supported by both experimental and theoretical data. Follow-up studies will aim to further validate these findings in cellular systems and to develop molecules with enhanced potency, selectivity, and pharmacological stability through structure-guided modification.

Author Contributions

Conceptualization, H.A.M.; methodology, H.A.M.; data curation, H.A.M.; formal analysis, H.A.M.; investigation, H.A.M.; writing—original draft preparation, H.A.M.; writing—review and editing, H.A.M. All authors have read and agreed to the published version of the manuscript.

Institutional Review Board Statement

Not applicable.

Informed Consent Statement

Not applicable.

Data Availability Statement

Data supporting the findings of this study are available upon reasonable request from the corresponding author.

Funding

The authors extend their appreciation to Prince Sattam bin Abdulaziz University for funding this research work through the project number (PSAU/2025/03/34701).

Acknowledgments

The authors are thankful to the Department of Pharmacology and Toxicology, College of Pharmacy, PSAU, for providing the facility to perform the study.

Conflicts of Interest

The author declares no conflict of interest.

References

1. Xie, Z.; Wu, B.; Liu, Y.; Ren, W.; Tong, L.; Xiang, C.; Wei, A.; Gao, Y.; Zeng, L.; Xie, H.; Tang, W.; Hu, Y. Novel class of colony-stimulating factor 1 receptor kinase inhibitors based on an o-aminopyridyl alkynyl scaffold as potential treatment for inflammatory disorders. *J. Med. Chem.* **2020**, *63*, 1397–1414, https://doi.org/10.1021/acs.jmedchem.9b01912.
2. Madkhali, H.; Tarawneh, A.; Ali, Z.; Le, H.V.; Cutler, S.J.; Khan, I.A.; Shariat-Madar, Z. Identification of human kinin-forming enzyme inhibitors from medicinal herbs. *Molecules* **2021**, *26*, 4126, https://doi.org/10.3390/molecules26144126.
3. Bork, K.; Meng, G.; Staubach, P.; Hardt, J. Hereditary angioedema: new findings concerning symptoms, affected organs, and course. *Am. J. Med.* **2006**, *119*, 267–274, https://doi.org/10.1016/j.amjmed.2005.09.064.
4. Joseph, K.; Ghebrehiwet, B.; Peerschke, E.I.; Reid, K.B.; Kaplan, A.P. Identification of the zinc-dependent endothelial cell binding protein for high molecular weight kininogen and factor XII: identity with the receptor that binds to the globular heads of C1q (gC1q-R). *Proc. Natl. Acad. Sci. U.S.A.* **1996**, *93*, 8552–8557, https://doi.org/10.1073/pnas.93.16.8552.
5. Schmaier, A.H. The contact activation and kallikrein/kinin systems: pathophysiologic and physiologic activities. *J. Thromb. Haemost.* **2016**, *14*, 28–39, https://doi.org/10.1111/jth.13194.
6. Farkas, H.; Stobiecki, M.; Peter, J.; Kinaciyan, T.; Maurer, M.; Aygören-Pürsün, E.; Kiani-Alikhan, S.; Wu, A.; Reshef, A.; Bygum, A. Long-term safety and effectiveness of berotralstat for hereditary angioedema: The open-label APeX-S study. *Clin. Transl. Allergy* **2021**, *11*, e12035, https://doi.org/10.1002/clt2.12035.
7. Oikonomopoulou, K.; Hansen, K.K.; Saifeddine, M.; Vergnolle, N.; Tea, I.; Diamandis, E.P.; Hollenberg, M.D. Proteinase-mediated cell signalling: targeting proteinase-activated receptors (PARs) by kallikreins and more. *Biol. Chem.* **2006**, *387*, 677-685, https://doi.org/10.1515/bc.2006.086.
8. Ran, X.; Zhang, Q.; Li, S.; Yu, Z.; Wan, L.; Wu, B.; Wu, R.; Li, S. Tissue kallikrein exacerbating sepsis-induced endothelial hyperpermeability is highly predictive of severity and mortality in sepsis. *J. Inflamm. Res.* **2021**, *14*, 3321-3333, https://doi.org/10.2147/JIR.S317874.
9. Xie, Z.; Li, Z.; Shao, Y.; Liao, C. Discovery and development of plasma kallikrein inhibitors for multiple diseases. *Eur. J. Med. Chem.* **2020**, *190*, 112137, https://doi.org/10.1016/j.ejmech.2020.112137.
10. Valerieva, A.; Longhurst, H.J. Treatment of hereditary angioedema: single or multiple pathways to the rescue. *Front. Allergy* **2022**, *3*, 952233, https://doi.org/10.3389/falgy.2022.952233.
11. Albert-Weißenberger, C.; Sirén, A.L.; Kleinschnitz, C. Ischemic stroke and traumatic brain injury: the role of the kallikrein-kinin system. *Prog. Neurobiol.* **2013**, *101–102*, 65–82, https://doi.org/10.1016/j.pneurobio.2012.11.004.
12. Chiș, A.; Noubissi, P.A.; Pop, O.-L.; Mureșan, C.I.; Fokam Tagne, M.A.; Kamgang, R.; Fodor, A.; Sitar-Tăut, A.-V.; Cozma, A.; Orășan, O.H. Bioactive compounds in Moringa oleifera: mechanisms of action, focus on their anti-inflammatory properties. *Plants* **2023**, *13*, 20, https://doi.org/10.3390/plants13010020.
13. Duan, L.; Cheng, S.; Li, L.; Liu, Y.; Wang, D.; Liu, G. Natural anti-inflammatory compounds as drug candidates for inflammatory bowel disease. *Front. Pharmacol.* **2021**, *12*, 684486, https://doi.org/10.3389/fphar.2021.684486.
14. Yamada, M.; Ono, K.; Hamaguchi, T.; Noguchi-Shinohara, M. Natural Phenolic Compounds as Therapeutic and Preventive Agents for Cerebral Amyloidosis. In Natural Compounds as Therapeutic Agents for Amyloidogenic Diseases, Vassallo, N., Ed.; Springer International Publishing: Cham, **2015**; Volume 863, pp. 79-94, https://doi.org/10.1007/978-3-319-18365-7_4.
15. Ito, R.; Statland, B.E. Centrifugal analysis for plasma kallikrein activity, with use of the chromogenic substrate S-2302. *Clin. Chem.* **1981**, *27*, 586–593, https://doi.org/10.1093/clinchem/27.4.586.
16. Li, Z.; Partridge, J.; Silva-Garcia, A.; Rademacher, P.; Betz, A.; Xu, Q.; Sham, H.; Hu, Y.; Shan, Y.; Liu, B. Structure-guided design of novel, potent, and selective macrocyclic plasma kallikrein inhibitors. *ACS Med. Chem. Lett.* **2017**, *8*, 185-190, https://doi.org/10.1021/acsmedchemlett.6b00384.
17. Liu H, Deng Y, Liu J, et al. Plasma Kallikrein Inhibitors for Multiple Disorders: Current Advances and Perspectives. *J Med Chem*. **2025**, 68, 21012-21034, https://doi.org/10.1021/acs.jmedchem.5c02234.

18. Madkhali, H.A.; Ansari, M.N.; Alamri, M.A. Inhibition of activated coagulation factor XII by the phosphodiesterase-4 inhibitor roflumilast: *in vitro* and *in silico* studies. *Front. Biosci.* **2025**, *30*, 38395, https://doi.org/10.31083/FBL38395.
19. 2. Frisch, M.J.; Trucks, G.W.; Schlegel, H.B.; Scuseria, G.E.; Robb, M.A.; Cheeseman, J.R.; Scalmani, G.; Barone, V.; Petersson, G.A.; Nakatsuji, H.; Li, X.; Caricato, M.; Marenich, A.V.; Bloino, J.; Janesko, B.G.; Gomperts, R.; Mennucci, B.; Hratchian, H.P.; Ortiz, J. V.; Izmaylov, A. F.; Sonnenberg, J.L.; Williams-Young, D.; Ding, F.; Lipparini, F.; Egidi, F.; Goings, J.; Peng, B.; Petrone, A.; Henderson, T.; Ranasinghe, D.; Zakrzewski, V.G.; Gao, J.; Rega, N.; Zheng, G.; Liang, W.; Hada, M.; Ehara, M.; Toyota, K.; Fukuda, R.; Hasegawa, J.; Ishida, M.; Nakajima, T.; Honda, Y.; Kitao, O.; Nakai, H.; Vreven, T.; Throssell, K.; Montgomery, J.A., Jr.; Peralta, J.E.; Ogliaro, F.; Bearpark, M.J.; Heyd, J.J.; Brothers, E.N.; Kudin, K.N.; Staroverov, V.N.; Keith, T.A.; Kobayashi, R.; Normand, J.; Raghavachari, K.; Rendell, A.P.; Burant, J.C.; Iyengar, S.S.; Tomasi, J.; Cossi, M.; Millam, J.M.; Klene, M.; Adamo, C.; Cammi, R.; Ochterski, J.W.; Martin, R.L.; Morokuma, K.; Farkas, O.; Foresman, J.B.; Fox, D.J. Gaussian 16, Revision C.01, Gaussian, Inc., Wallingford CT, **2016**.
20. Lu, T.; Chen, F. Multiwfn: a multifunctional wavefunction analyzer. *J. Comput. Chem.* **2012**, *33*, 580–592, https://doi.org/10.1002/jcc.22885.
21. Humphrey, W.; Dalke, A.; Schulten, K. VMD: visual molecular dynamics. *J. Mol. Graph.* **1996**, *14*, 33–38, https://doi.org/10.1016/0263-7855(96)00018-5.
22. Contreras-García, J.; Johnson, E.R.; Keinan, S.; Chaudret, R.; Piquemal, J.-P.; Beratan, D.N.; Yang, W. NCIPLOT: a program for plotting non-covalentt interaction regions. *J. Chem. Theory Comput.* **2011**, *7*, 625-632, https://doi.org/10.1021/ct100641a.
23. Trott, O.; Olson, A.J. AutoDock Vina: improving the speed and accuracy of docking with a new scoring function, efficient optimization, and multithreading. *J. Comput. Chem.* **2010**, *31*, 455–461, https://doi.org/10.1002/jcc.21334.
24. Schrödinger, L. The PyMOL Molecular Graphics System, Version 1.8. **2015**.
25. BIOVIA Discovery Studio; Dassault Systèmes: San Diego, CA, USA, **2016**.
26. Abraham, M.J.; Murtola, T.; Schulz, R.; Páll, S.; Smith, J.C.; Hess, B.; Lindahl, E. GROMACS: high performance molecular simulations through multi-level parallelism from laptops to supercomputers. *SoftwareX* **2015**, *1–2*, 19–25, https://doi.org/10.1016/j.softx.2015.06.001.
27. Huang, J.; Rauscher, S.; Nawrocki, G.; Ran, T.; Feig, M.; De Groot, B.L.; Grubmüller, H.; MacKerell Jr, A.D. CHARMM36m: an improved force field for folded and intrinsically disordered proteins. *Nat. Methods* **2017**, *14*, 71-73, https://doi.org/10.1038/nmeth.4067.
28. Daina, A.; Michielin, O.; Zoete, V. SwissADME: a free web tool to evaluate pharmacokinetics, drug-likeness and medicinal chemistry friendliness of small molecules. *Sci. Rep.* **2017**, *7*, 42717, https://doi.org/10.1038/srep42717.
29. Xiong, G.; Wu, Z.; Yi, J.; Fu, L.; Yang, Z.; Hsieh, C.; Yin, M.; Zeng, X.; Wu, C.; Lu, A. ADMETlab 2.0: an integrated online platform for accurate and comprehensive predictions of ADMET properties. *Nucleic Acids Res.* **2021**, *49*, W5-W14, https://doi.org/10.1093/nar/gkab255.
30. Ait Elmachkouri, Y.; Rajesh, R.; Altharawi, A.; Frit, A.A.; Alossaimi, M.A.; Riadi, Y.; Aldakhil, T.; Taha, M.L.; Haggam, R.A. Synthesis, molecular structure, spectroscopic, electronic properties, molecular docking, and molecular dynamics studies on novel 1,2,3-triazole-thiosemicarbazone: a potent breast cancer drug. *Comput. Biol. Chem.* **2025**, *119*, 108580, https://doi.org/10.1016/j.compbiolchem.2025.108580.
31. Ait Elmachkouri, Y.; Irrou, E.; Ouachtak, H.; Zaki, M.E.A.; Gomha, S.M.; Oubella, A.; Alotaibi, S.H.; Taha, M.L. *In silico* studies of pyrazolopyranopyrimidine as a potential anticancer inhibitor: synthesis, network pharmacology, ADMET prediction, molecular docking, and dynamics simulations. *J. Mol. Struct.* **2025**, *1343*, 142829, https://doi.org/10.1016/j.molstruc.2025.142829.
32. Ait Elmachkouri, Y.; Irrou, E.; Yamari, I.; Chtita, S.; Toubi, Y.; AlAjmi, M.F.; Taha, M.L. Synthesis, crystal structure, anticancer activity, and computational studies of novel pyrazolo[4′,3′:5,6]pyrano[2,3-d]pyrimidine derivatives as potential anticancer agents. *Future Med. Chem.* **2025**, *17*, 2101–2118, https://doi.org/10.1080/17568919.2025.2552641.

Publisher's Note & Disclaimer